A Fast 3-D Numerical Impedance Calculation for Litz Wire and Air-Core Coils

Tianming Luo, *Member, IEEE*, Mohamad Ghaffarian Niasar, *Member, IEEE*, and Peter Vaessen, *Member, IEEE*

***Abstract*—This article presents a 3-D numerical impedance calculation method based on cylindrical elements. It can be used to model the Litz wire and further air-core coil wound by the Litz wire. The discretization is based on cylindrical elements, resulting in a small amount of elements. Cylindrical element analysis is based on a 2-D analysis and its analog to 3-D. The analysis considers both transverse and longitudinal magnetic fields applied to elements. The proposed method is applied to several Litz wires and compared with 3-D finite element method (FEM), which validates that the method has good accuracy and fast computational speed. The effectiveness of the method for the air-core coil is validated by measurements. The proposed method is promising in facilitating coil optimization.**

***Index Terms*—Air-core coil, copper losses, eddy current, Litz wire, proximity effect, skin effect.**

I. Introduction

AIR-CORE magnetic components are a promising alternative extending the gravimetric power density limit [1], [2]. Without magnetic material, the losses of magnetic components are from windings, shields, and accessories, and winding loss is dominant [2]. In medium-frequency applications, Litz wire is a common choice. Therefore, an impedance calculation method for windings wound by Litz wire is essential for this application.

Litz wires can dramatically reduce the eddy current losses through twisting. However, it leads to complex structures and difficulties in calculation. Generally, the 3-D finite element method is a common choice, but the computational cost is high [3]. For simplicity, it is common to assume a perfect twisting, which leads to uniform current in each strand and consider only the strand-level effect [4], [5], [6]. However, perfect twisting requires that each strand is evenly spatial distributed radially and azimuthally along the entire length of the wire. This is hard to achieve for actual Litz wires, which makes the bundle-level effects considerable [7], [8]. Various methods have been developed to increase the computational speed. The 2.5-D approximation [9], [10] is developed to approximate the 3-D cases by several 2-D simulations. PEEC is a promising numerical method approximating the field problem with an electrical equivalent circuit [11], [12]. In [11], the combination of cylindrical elements and formulas from [4] reduces the discretization effort, which assumes a uniform magnetic field across the cross section of strands and neglects the impact of eddy current on magnetic field at the same time.

There are two often used methods for windings wound by Litz wires. One uses ac resistance R_{ac} and proximity effect factor G based on perfect twisting assumption in winding models [13]. Another is the homogenization method [14], [15], which extracts effective complex permeability of Litz wire and models windings with finite element method (FEM).

Compared to focusing on the impedance calculation of Litz wires or coils alone, this article presents a 3-D numerical impedance calculation method, which can calculate the impedance from a pitch of Litz wires to air-core coils wound by Litz wires. The proposed method adopts cylindrical elements, the same as [11]. It leads to a small amount of elements. Rather than only using formulas from [4], the proposed method considers longitudinal and transverse magnetic fields applied on each element. The analysis for transverse magnetic field is based on the 2-D analysis in [16] and is extended to 3-D through analog. After obtaining the impedance matrices of Litz wires, the representative parameters are extracted and form equivalent cylindrical elements used in coil models. The proposed method can quickly and accurately calculate the impedance in the broader frequency range and is promising in facilitating Litz wire and coil optimization.

The rest of this article is organized as follows. Section II introduces the basic theory for the proposed method. It includes the analysis of cylindrical elements under a quasi-static magnetic field, the circuit analysis of Litz wires, and coupling air-core coils and Litz wires. Section III validates the proposed method for Litz wires and air-core coils by comparing it with other methods and measurements. Finally, Section IV concludes this article.

II. Basic Theory of the Proposed Method

This section introduces the basic theory of the proposed method. It consists of further three sections. Section II-A introduces the analysis of cylindrical elements under a quasi-static

Received 5 August 2024; revised 11 October 2024; accepted 22 November 2024. Date of publication 27 November 2024; date of current version 26 December 2024. This work was supported by China Scholarship Council under Grant 202007720032. Recommended for publication by Associate Editor M. Chen. *(Corresponding author: Tianming Luo.)*

Tianming Luo and Mohamad Ghaffarian Niasar are with the Department of Electrical Sustainable Energy, Delft University of Technology, 2628CD Delft, The Netherlands (e-mail: T.Luo-1@tudelft.nl; m.ghaffarianniasar@tudelft.nl).

Peter Vaessen is with the Department of Electrical Sustainable Energy, Delft University of Technology, 2628CD Delft, The Netherlands, and also with the KEMA laboratories, Arnhem, The Netherlands (e-mail: p.t.m.vaessen@tudelft.nl).

Color versions of one or more figures in this article are available at https://doi.org/10.1109/TPEL.2024.3507368.

Digital Object Identifier 10.1109/TPEL.2024.3507368

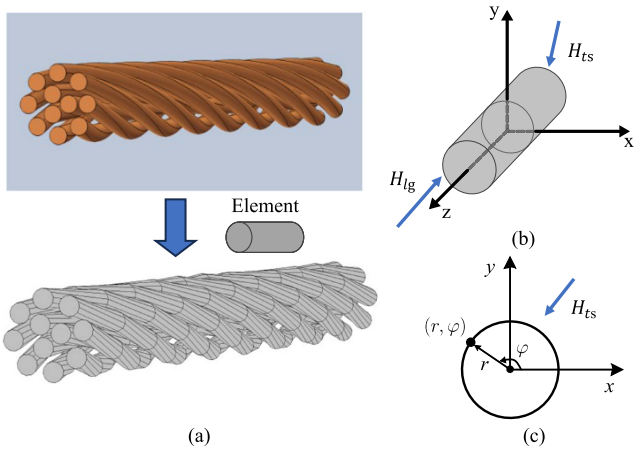

Fig. 1. (a) Illustration of Litz wire discretization with cylindrical elements. (b) Illustration of transverse and longitudinal magnetic fields on an element in 3-D Cartesian coordinates. (c) Illustration of the transverse field in polar and 2-D Cartesian coordinates.

magnetic field, which explains how each element interacts. Then, Section II-B introduces the impedance analysis of Litz wires. It clarifies the composition of ac resistance in Litz wires. Section II-C presents the equivalent cylindrical element representing Litz wires and its application in air-core coils.

A. Analysis of Cylindrical Elements

In the proposed method, Litz wires or coils are discretized with cylindrical elements, as shown in Fig. 1(a). A strand is composed of several series connecting cylindrical elements. Therefore, the analysis of cylindrical elements is the basis of the method. There are two adopted assumptions to simplify the problem. The first one is that the current flows along the paths of strands. The next is the independence between eddy currents caused by transverse and longitudinal magnetic fields, as shown in Fig. 1(b). Therefore, the 3-D magnetic field problem becomes two 2-D field problems for each cylindrical element.

1) Transverse Magnetic Field: A large magnetic field applied along the coil is uncommon in magnetic components. Therefore, transverse magnetic field H_{ts} is the main factor causing eddy current in cylindrical elements. The analysis is first derived in 2-D and then extended to 3-D. The 2-D analysis is based on the analysis in [16], briefly summarized here, and the more detailed derivation is given in the Appendix. As Fig. 1(c) shows, the 2-D analysis is done in the polar and 2-D Cartesian coordinates, whose original points are the center of the transverse cross section of elements. In polar coordinates, the general solution of the magnetic vector potential A around elements is described by the following equation:

$$\nabla^2 A(r, \varphi) = 0. \tag{1}$$

For the transverse field analysis in this article, the general solution of the magnetic vector potential A only considers the constant and first-order harmonic terms, as shown in (2). The coefficient C is the vector potential contributed by currents in other elements, coefficient D relates to the net current I flowing in the element, and coefficients A', A'', B', and B'' relate to the first-order harmonics

$$A(r, \varphi) = C + D \ln(r) + \left(rA' + \frac{A''}{r}\right)\cos(\varphi) + \left(rB' + \frac{B''}{r}\right)\sin(\varphi). \tag{2}$$

Based on the boundary condition on the surface of the element, i.e., the continuity of magnetic vector potential, normal term of the flux density, and tangential term of the magnetic field, the relations between coefficients in (2) can be derived, which are given in (3). The J_n is the first kind of Bessel function; the subscript n is the order, a is the element's radius, and κ relates to skin depth

$$D = -\frac{\mu_0 I}{2\pi} \quad A_1''|B_1'' = \frac{a^2 J_2(\kappa a)}{J_0(\kappa a)} A_1'|B_1'$$
$$\kappa^2 = -j\omega\sigma\mu. \tag{3}$$

When there are multiple circular elements, each element has a magnetic vector potential solution in the form of (2), with each function expressed in the polar coordinates of the corresponding element. The functions are converted into 2-D Cartesian coordinates. Since the value of the Green's function for the Laplace equation is reserve proportional to distance, (2) is separated into two parts based on the relation between value and distance. Part one consists of coefficients D, A'', and B'', which are generated from the source inside the element. Part two consists of other coefficients generated from the source outside the element. After matching part two of an element and part one from the other elements in the same coordinates, a relation like (4) can be built. Subscripts i and j denote different conductors. The x_{ji} and y_{ji} are the coordinate changes from j to i element in the x and y coordinates. Through solving the matrix, the coefficients under 2-D situations can be obtained

$$\begin{aligned}
C_i + \sum_{j\neq i} A_j'' \frac{x_{ji}}{x_{ji}^2 + y_{ji}^2} + \sum_{j\neq i} B_j'' \frac{y_{ji}}{x_{ji}^2 + y_{ji}^2} &= \sum_{j\neq i} \frac{D_j}{2} \ln(x_{ji}^2 + y_{ji}^2) \\
A_i' + \sum_{j\neq i} A_j'' \frac{x_{ji}^2 - y_{ji}^2}{(x_{ji}^2 + y_{ji}^2)^2} + \sum_{j\neq i} B_j'' \frac{2x_{ji}y_{ji}}{(x_{ji}^2 + y_{ji}^2)^2} &= \sum_{j\neq i} D_j \frac{x_{ji}}{x_{ji}^2 + y_{ji}^2} \\
B_i' + \sum_{j\neq i} A_j'' \frac{2x_{ji}y_{ji}}{(x_{ji}^2 + y_{ji}^2)^2} - \sum_{j\neq i} B_j'' \frac{x_{ji}^2 - y_{ji}^2}{(x_{ji}^2 + y_{ji}^2)^2} &= \sum_{j\neq i} D_j \frac{y_{ji}}{x_{ji}^2 + y_{ji}^2}.
\end{aligned} \tag{4}$$

Then, the matrix needs to be extended to 3-D situations. The coefficient D in (4) is replaced by current I based on the relation given in (3). The physical meanings of the right-hand side of (4) are the magnetic vector potential A, and the flux density $-B_y$, B_x at the center of element i induced by the current

in element j in 2-D dc situations, respectively. Besides, the geometric components of A_j'' and B_j'' terms in the first equation of (4) are identical to the geometric components of the flux density $-B_y$, B_x terms. Therefore, these three geometric parts in the matrix (4) are replaced by the Biot–Savart law in 3-D situations. Equation (5) provides the differential of the flux density B_y, B_x, which are used to integral along elements. The physical meanings of these terms in 3-D are the same as those in 2-D

$$dB_x = -\frac{\mu_0 I}{4\pi}\frac{y}{(x^2+y^2+z^2)^{3/2}}$$
$$dB_y = \frac{\mu_0 I}{4\pi}\frac{x}{(x^2+y^2+z^2)^{3/2}}. \tag{5}$$

Then, there are still two geometric components related to A_j'' and B_j'' in the second and third equations of (4). The corresponding 3-D terms are needed. To have the same physical meaning, the integration of 3-D terms over the z-axis should result in the geometric components in the 2-D. Through analogy, the differentials of two variables are obtained in (6). These differentials are used to perform integration along elements. All terms in the 3-D version of (4) are known. Besides, for simplicity, the formulas (5) and (6) are based on the current I along the z-axis. Since each cylindrical element has its direction, simple coordinate conversions are needed to unify all terms in the same coordinates

$$dG_x = \frac{3xy}{2(x^2+y^2+z^2)^{5/2}} \int_{z=-\infty}^{z=\infty} \mathrm{d}G_x = \frac{2xy}{(x^2+y^2)^2}$$
$$dG_y = \frac{3(x^2-y^2)}{4(x^2+y^2+z^2)^{5/2}} \int_{z=-\infty}^{z=\infty} \mathrm{d}G_y = \frac{x^2-y^2}{(x^2+y^2)^2}. \tag{6}$$

Therefore, a matrix describing the relationships of the transverse field between cylindrical elements can be constructed. After solving the matrix, each element's coefficients in (2) are obtained. The relationship between cylindrical elements' physical quantities and mathematical coefficients also uses the relationship in 2-D situations. The relation between potential ϕ, current I, and $\bar{A}$ is given in (7), where $\bar{A}$ is the average vector potential A over the cross section of an element

$$-\nabla\phi = R_{\mathrm{dc}} I + j\omega\bar{A}. \tag{7}$$

The $\bar{A}$ is given in (8). The derivation is given in the Appendix. Combining (7) and (8), the potential of each element can be obtained

$$\bar{A} = C + D\ln(a) - \frac{DJ_2(\kappa a)}{\kappa a J_1(\kappa a)}. \tag{8}$$

Compared to the methods that assume a uniform external field, the most significant difference is whether to consider the interaction of eddy current. It is reflected in the last two equations in (4). Since a fixed relationship exists between A_i', B_i' and A_i'', B_i'', the coefficients A_i' and B_i' can represent the field around the circular element i. For methods assuming a uniform field, coefficients A_i' and B_i' are directly equal to the right-hand side of the equation, i.e., flux density $-B_y$, B_x, and do not influence the other A_j' and B_j'. Then, the coefficient C is obtained based on the first equation in (4), and the average magnetic vector potential $\bar{A}$ can be obtained. However, when the summation of contribution from A_j'' and B_j'' terms are comparable with the flux density, it leads to a considerable error in the average magnetic vector potential $\bar{A}$. The error is finally reflected in the winding loss, such as the significant error of Ferreira's formula in compact windings at high frequency [17]. Therefore, the method used in this article can more accurately model the transverse magnetic field effect for each element.

Of course, when the summation of contribution from A_j'' and B_j'' terms are negligible, the uniform transverse external field assumption is satisfied, and the contributions of the proximity effect to impedance can be obtained by a simple equation (9). H_{ik} and H_{jk} are the transverse fields applied on element k caused by 1 A current in strand i and j, respectively. The k can denote all elements. Subsequently, an approximate Z_{ts} for low frequencies is obtained

$$Z_{\mathrm{ts\_p}ij} = -\frac{2\pi\kappa^2 a^2 J_2(\kappa a)}{\sigma J_0(\kappa a)} \sum_k H_{ik}\cdot H_{jk}. \tag{9}$$

2) Longitudinal Magnetic Field: In many Litz wire models, longitudinal magnetic field H_{lg} is often neglected because of its trivial field strength when the wires have a relatively long pitch. Here, the term associated with the longitudinal magnetic field is added to double-check the assumption. By solving a round conductor subjected to a uniform longitudinal field in 2-D, (10) is obtained by integrating the Poynting vector over the perimeter. The real part of S is the loss, and the imaginary part is the reactive power. If $H_{\mathrm{lg}-ik}$ and $H_{\mathrm{lg}-jk}$ are longitudinal fields applied to k caused by a unit current in i and j elements, the impedance Z_{lg_ij} is calculated with (11). The impact of the generated eddy current is neglected

$$S = -\frac{2\pi\kappa a J_1(\kappa a)}{\sigma J_0(\kappa a)} H_{\mathrm{lg}}^2 \tag{10}$$
$$Z_{\mathrm{lg}\_ij} = -\frac{2\pi\kappa a J_1(\kappa a)}{\sigma J_0(\kappa a)} \sum_k H_{\mathrm{lg}\_ik}\cdot H_{\mathrm{lg}\_jk}. \tag{11}$$

B. Litz Wires' Equivalent Circuit

Based on the analysis of cylindrical elements, if the currents in elements are known, the potential of elements can be solved. However, due to the imperfect twisting, knowing the current distribution among strands is a problem. Impedance matrices are a good option for obtaining the current distribution. Therefore, this section introduces the Litz wires' equivalent circuit and how to convert the variables in Section II-A into circuit elements.

The impedance matrices can be generalized into (12); $\mathbf{Z}_{ss}$ is the impedance matrix among the strands, $\mathbf{Z}_{sw}$ characterizes the voltage induced by a unit external magnetic field, and $\mathbf{Z}_{ww}$ characterizes the energy consumed in the Litz wire caused by a unit external magnetic field. $\mathbf{Z}_{ws}$ represents the impact of current in strands on the source of external magnetic fields

$$\mathbf{Z}_{\mathrm{Litz}} = \begin{pmatrix} \mathbf{Z}_{ss} & \mathbf{Z}_{sw} \\ \mathbf{Z}_{ws} & \mathbf{Z}_{ww} \end{pmatrix}. \tag{12}$$

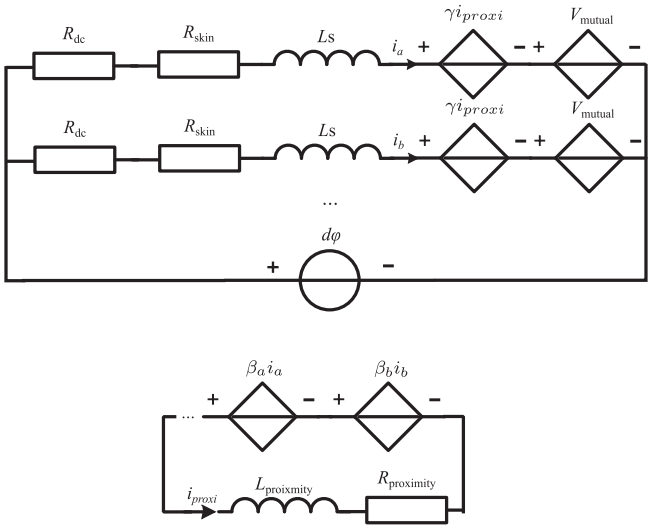

Fig. 2. Equivalent circuit of Litz wire.

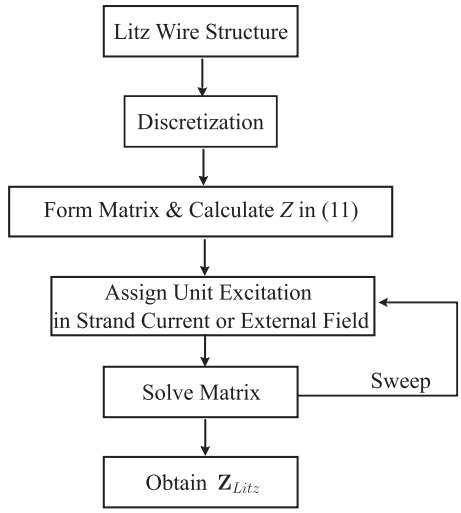

Fig. 3. Flowchart for calculating the impedance matrix of Litz wires.

First, the $\mathbf{Z}_{ss}$ is analyzed, and the size of it is $n_s \times n_s$, where n_s is the number of strands. The n row m column element in $\mathbf{Z}_{ss}$ represents the relationship between strands n and m. Fig. 2 shows the equivalent circuit of strands. Each strand has the same potential drop. Each strand's circuit elements can be separated into two parts.

The first part is the elements decided by the strand itself, involving dc resistance R_{dc}, resistance due to skin effect R_{skin}, and self-inductance L_{s}. This part only contributes to the elements on the main diagonal of $\mathbf{Z}_{ss}$. From the cylindrical element point of view, it is represented by R_{dc} in (7) and D related terms in (8). Since the current is the same for all cylindrical elements in a strand, this part is the summation of the production of the impedance of unit length and l_k for the elements in a strand, as shown in (13), where l_k is the length of element k

$$Z_{\text{self}-n} = \sum_{k\in n}\left(R_{\text{dc}} - \frac{\mu_0}{2\pi}\left(\ln a - \frac{J_2(\kappa a)}{\kappa a J_1(\kappa a)}\right)\right) l_k. \quad (13)$$

The second part relates to the mutual effect between strands involving two dependent voltage sources. One voltage source V_{mutual} is induced by mutual inductance, and the other is γi_{proxi}, which is caused by the proximity effect. Mutual inductance contributes to the nondiagonal elements in $\mathbf{Z}_{ss}$. The right-hand side of the equation in the first row of (4) represents the magnetic vector voltage in element i caused by j and is denoted by $A_{\text{mut}L-ij}$ for simplicity. The impedance due to mutual inductance is given in the following equation:

$$Z_{\text{mut}L-nm} = \sum_{i\in n}\sum_{j\in m} j\omega \frac{A_{\text{mut}L-ij}}{I_m}. \quad (14)$$

The γi_{proxi} depends on the current i_{proxi} in the second circuit. The magnetic field induces potential difference, which leads to the proximity effect. The dependent voltage sources βi represent the magnetic fields caused by currents i in strands. The impedance calculation, compared to the previous two parts, is more complex and requires to solve the matrix built in Section II-A and (10). Set the current in m as 1 A and others as 0 A. Then, a matrix can be formed ignoring the right-hand side of the equation in the first row of (4), which is already considered in (14). Through solving the matrix, the variable C of each element can be obtained. Sum the variable C belonging to n together, and the part of γi_{proxi} in strand n is obtained, which is caused by 1 A in m, and equal to the impedance caused by the transverse magnetic field. The longitudinal field's contribution is calculated through (11). The impedance due to proximity effect is given in (15). The $\mathbf{Z}_{ss}$ is the summation of $Z_{\text{self}-n}$, $Z_{\text{mut}L-nm}$, and $Z_{\text{proxi}-nm}$

$$Z_{\text{proxi}-nm} = \sum_{i\in n} j\omega C_i + \sum_{i\in n}\sum_{j\in m}\sum_{k} Z_{\text{lg}\_ij}. \quad (15)$$

Then, the matrices $\mathbf{Z}_{sw}$ and $\mathbf{Z}_{ww}$ are analyzed. These two submatrices are caused by external magnetic fields. The size of $\mathbf{Z}_{sw}$ is $n_s \times 3$, and the size of $\mathbf{Z}_{ww}$ is 3×3. Columns represent external fields along x, y, and z directions. The $\mathbf{Z}_{sw}$ and $\mathbf{Z}_{ww}$ are also represented by the two dependent voltage sources V_{mutual} and γi_{proxi} in the circuit. The value is also calculated with the same method for $Z_{\text{mut}L-nm}$ and $Z_{\text{proxi}-nm}$. The currents in all strands are set to 0 A, and an additional element producing an external field of 1 A/m is introduced. The $\mathbf{Z}_{ws}$ is ignored since it can be replaced by $\mathbf{Z}_{sw}$ for another section of the coil.

Fig. 3 shows the flowchart for calculating the Litz wires' impedance matrix. After building the matrix based on the method in Section II-A, the impedance matrix $\mathbf{Z}_{ss}$ can be calculated by sweeping the Litz wire strands with a unit current while others carry zero current. Then, $\mathbf{Z}_{sw}$ and $\mathbf{Z}_{ww}$ are obtained by sweeping the unit external fields in x, y, and z dimensions and solving the matrix. To consider the impact of external fields, i.e., they are also swept to obtain three more dimensions in the impedance matrix.

C. Equivalent Cylindrical Element

Although it is possible to model the whole coil at the strand level, it requires considerable computational resources,

especially for multiturn coils. In this section, an equivalent cylindrical element is introduced to facilitate calculation.

In the homogenization technique, complex permeability is often used to approximate the proximity effect [14], [18], [19]. This technique can speed up the computation because it does not need a fine mesh for eddy current and reduces the number of elements. The complex permeability of an isolated round conductor is calculated under a uniform field with different frequencies. The equivalent complex permeability $\dot{\mu_{rc}}$ is given in (16), which is equal to the formula given in [19]. The value is valid when the field is nearly uniform because the complex permeability is derived based on the uniform external field situation. Then, the complex permeability is used in the winding region, and the magnetic energy under a static magnetic field is calculated. Next, the losses due to the proximity effect are approximated by the total magnetic energy times $j\omega$. The skin effect is calculated independently with an analytical method

$$\dot{\mu}_{rc} = \mu_{rc}\frac{J_0(\kappa a) + J_2(\kappa a)}{J_0(\kappa a) - J_2(\kappa a)}. \tag{16}$$

The equivalent cylindrical element adopts the key idea, which is using a simplified element with equivalent properties to replace the initial domain. Then, coils are discretized by the equivalent cylindrical elements, and the impedance can be calculated in a similar way as the method in Section II-B. To use the equivalent cylindrical elements, the required parameters need to be extracted from the Litz wire model.

The noninteger pitch length Litz wire can have a larger loss because it leads to unequal induced voltages in $\mathbf{Z}_{sw}$ and generates circulating currents to balance the voltage on the ends. However, for Litz wires, the induced voltages are needed to accumulate along the whole windings, which is much longer than a pitch. Then, the few voltages induced by the noninteger pitch meet the accumulated $\mathbf{Z}_{ss}$ and only cause negligible circulating current. Therefore, the properties of the equivalent element are extracted from the impedance matrix of one pitch of the Litz wire.

Based on the impedance matrices (12), the parameters of the equivalent element can be obtained as follows steps. First, the equivalent impedance, which is only related to the Litz wire itself, is calculated by the total strand current under a unit voltage drop. Strand currents are obtained based on the $\mathbf{Z}_{ss}$, as given in (17), where U is an $n_s \times 1$ unit voltage vector. The equivalent impedance $\dot{Z}_s$ works as the $Z_{\text{self}-n}$ in coil models

$$\dot{Z}_s = 1/\sum \mathbf{Z}_{ss}^{-1}U. \tag{17}$$

The second part, $\mathbf{Z}_{sw}$, is used to calculate the impact of the potential circulating current. The difference in voltage drop V_{ind} on each strand is obtained by accumulating field-weighted induced voltage. The circulating current I_{ind} and its impedance Z_{ind} can be calculated, as shown in (18). The H_k is the magnetic field matrix on the kth equivalent element with $n_s \times 3$ size, which is caused by a unit current in the coil. The l_k is the length of the kth equivalent element. The impedance Z_{ind} is an additional impedance, which is not used in the method in Section II-B. Therefore, it is added to the impedance obtained from the equivalent elements and the method in Section II-B. The impact of the circulating current on magnetic field distribution is not considered

$$\begin{aligned} V_{\text{ind}} &= \mathbf{Z}_{sw}\sum_k H_k l_k \\ I_{\text{ind}} &= \left(\mathbf{Z}_{ss}\sum_n l_n\right)^{-1} V_{\text{ind}} \\ Z_{\text{ind}} &= -V_{\text{ind}} I_{\text{ind}}^*/(1\text{A})^2. \end{aligned} \tag{18}$$

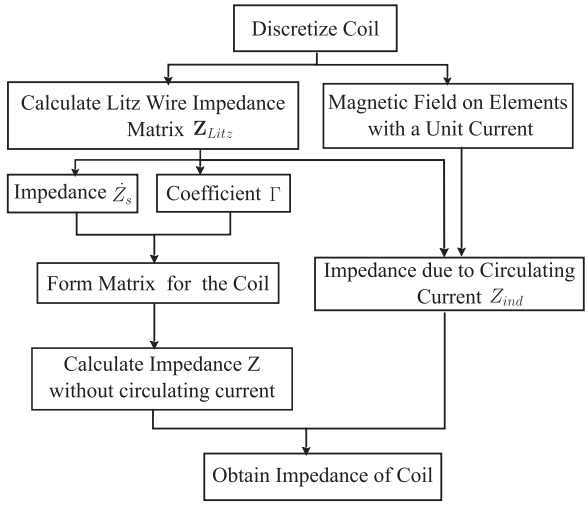

Fig. 4. Flowchart for calculating the impedance of air-core coil.

The last part is about $\mathbf{Z}_{ww}$. It reflects the impact of external fields, which are given in (9) and (11). For equivalent cylindrical elements, the field is also divided into transverse and longitudinal fields. For longitudinal fields, the value in $\mathbf{Z}_{ww}$ representing the impact of the z-direction field is used to replace the term before the summation symbol in (11). For transverse field analysis, the coefficient representing the relationship between $A''|B''$ and $A'|B'$ is important. The change of the energy due to a uniform external field is given in (19), and its real part is the proximity loss of a round conductor under a uniform external field. Combining (3) and (19), the coefficient Γ for the relationship between $A''|B''$ and $A'|B'$ of the equivalent element is given in (20)

$$UI = 2j\omega\pi\mu_0\frac{A_1''}{A_1'}H^2 = 2j\omega\pi\mu_0 a^2\frac{J_2(\kappa a)}{J_0(\kappa a)}H^2 \tag{19}$$

$$\Gamma = \frac{\dot{A}_1''}{\dot{A}_1'} \text{ or } \frac{\dot{B}_1''}{\dot{B}_1'} = \frac{\mathbf{Z}_{ww}}{2j\omega\pi\mu_0}. \tag{20}$$

Among the three considered parts, $\dot{Z}_s$ and Γ are the properties for a single element. Z_{ind} is decided by the whole coil. After obtaining the properties of the equivalent element, the impedance of an air-core coil can be calculated. The procedure is given in Fig. 4. First, the coil is discretized with equivalent elements. Then, the impedance matrix of the used Litz wire is obtained based on the procedure in Fig. 3. Extract the properties for equivalent elements based on the procedure in this section. The last step is forming the impedance matrix based on the equivalent element and calculating the coil's impedance.

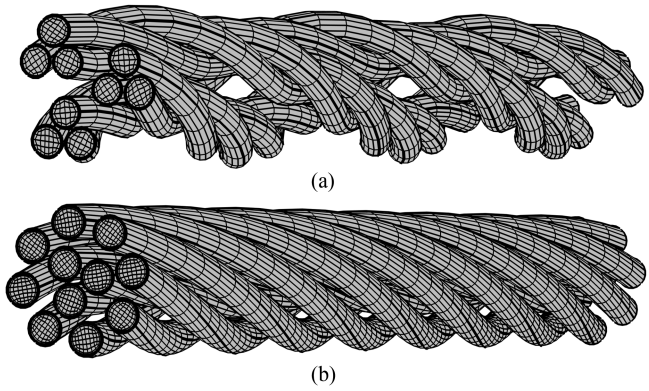

Fig. 5. Structures and FEM meshes of two cases. (a) Case 1. (b) Case 2.

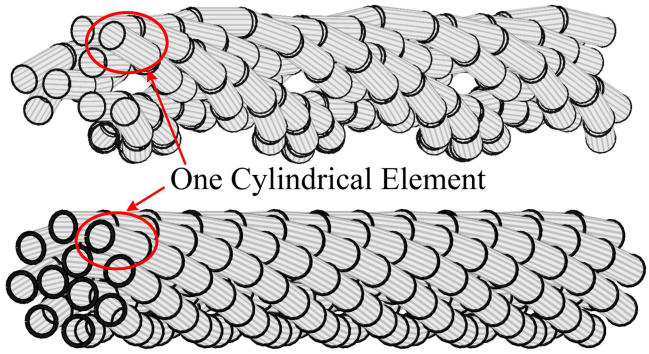

Fig. 6. Two cases with cylindrical elements.

III. Modeling and Validation

This section first introduces settings in modeling Litz wires and then validates the method for Litz wires. Then, the equivalent cylindrical element is validated by measuring the impedance of an air-core coil sample. The results are also compared with other methods.

A. Litz Wire

The prerequisite of the proposed method is the known structure. In this article, the structure of Litz wire is built with a recursive multilevel bundle structure [3]. To validate the proposed method for Litz wire, 3-D FEMs with COMSOL are set as the reference. To guarantee accuracy, boundary elements are adopted, and the size of the elements in the strands' cross section is made smaller than the skin depth.

Two different kinds of cases were calculated. Case 1 comprises nine strands, structured as 3×3 two-level bundles. Each strand is twisted in both radial and azimuthal directions. Case 2 comprises 11 strands without subbundle, which are only twisted in the radial direction. The strands radius, insulation layer thickness, and pitch of the top-level bundle are the same for both cases, which are 0.1, 0.01, and 10 mm, respectively. The structures and mesh in 3-D FEMs are shown in Fig. 5.

Fig. 6 illustrates how cylindrical elements model the two cases. The number of cylindrical elements is much smaller than the number of mesh in FEM. Since the number of elements in

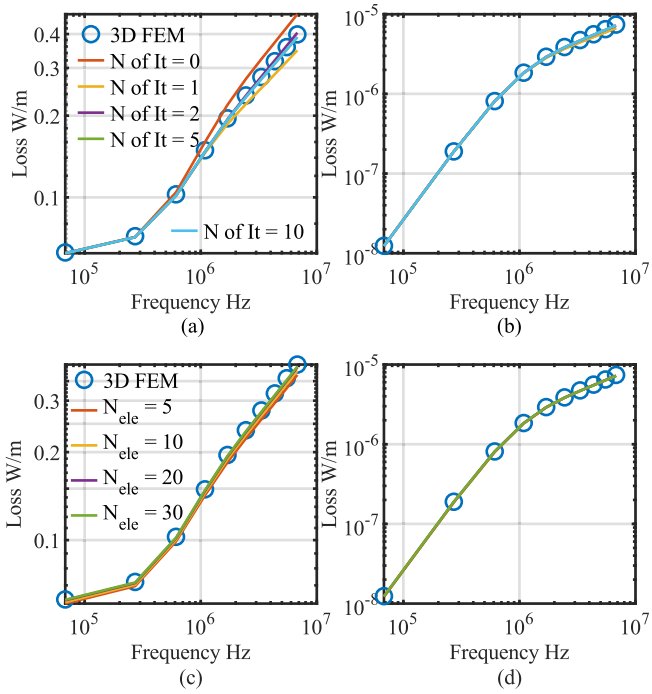

Fig. 7. Impact of iteration and element size on the results of case (1).

3-D Litz wire models can be large, the size of matrices built according to Fig. 3 can be considerable. Therefore, iteration methods can be used to solve the matrices to achieve fast computational speed. The initial values use the outcomes under a static magnetic field. Therefore, there are two factors that can impact the result: one is the element size, and another is the number of iterations. Fig. 7 shows the results of the case (1) with different element sizes and iteration numbers. Fig. 7(a) and (b) shows the results of the loss due to 1 A excitation current and 1 A/m external magnetic field under different iteration numbers, respectively. From the figure, it is known that the results converge fast, and five iterations are enough to reach convergence in general. The element size is represented by the number of elements in each strand. Its impact is not significant according to Fig. 7(c) and (d). Because the cases' structure is not complicated, each strand comprises 20 elements.

After deciding the setting of models, two cases are calculated with the proposed method, 3-D FEM, perfect twisting model [4] and the uniform field method. The uniform field represents the situations that do not consider the impact of the eddy current and the longitudinal field. It is theoretically the same as [11].

Case (1) is twisted in both radial and azimuthal directions, which leads to a roughly average current distribution in each strand. It is supposed to have a uniform current distribution. Fig. 8(a) and (c) shows the loss due to 1 A excitation current. The perfect twisting model exhibits good accuracy compared to 3-D FEM because the case aligns with the model's assumption. The uniform field gives good accuracy in the low-frequency range. With increasing frequency, the impact of eddy current cannot be ignored and gradually results in considerable error. The result considering the longitudinal field is slightly more accurate than the result that does not consider the longitudinal field. Fig. 8(c)

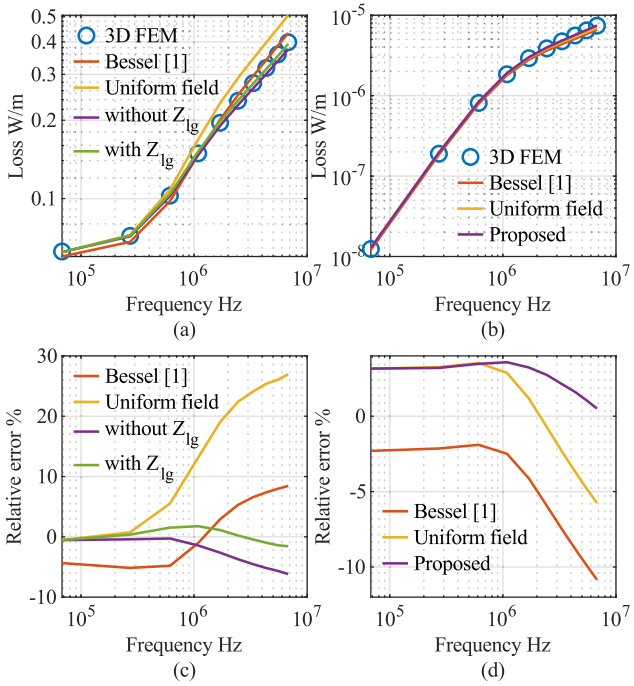

Fig. 8. Case (1): Loss per meter caused by (a) 1 A excitation current and (c) relative error; loss per meter caused by (b) 1 A/m external magnetic field and (d) relative error.

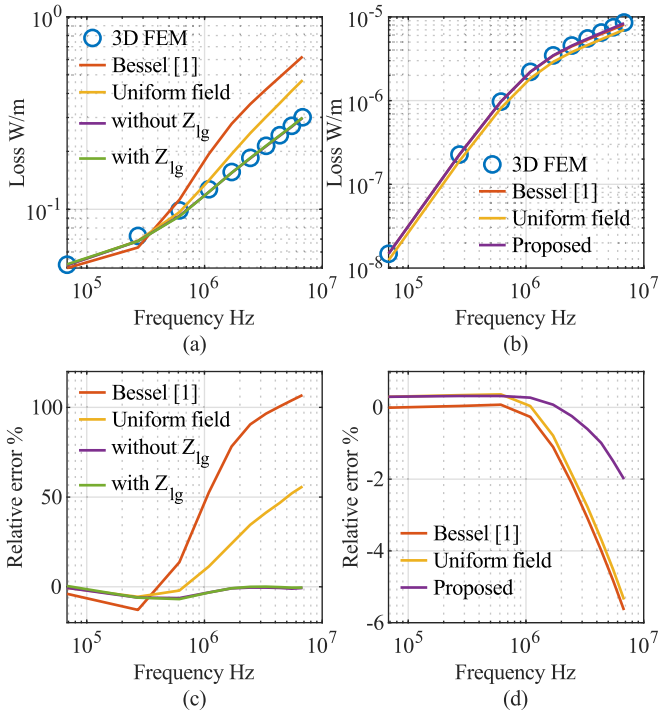

Fig. 9. Case (2): Loss per meter caused by (a) 1 A excitation current and (c) relative error; loss per meter caused by (b) 1 A/m external magnetic field and (d) relative error.

and (d) shows the loss due to the external magnetic field and the error compared to 3-D FEM. With rising frequency, the error increases. The proposed method keeps the error within 5% in the large frequency range.

Case (2) is only twisted in the azimuthal direction and should have a current distribution problem. As shown in Fig. 9(a) and (c), the perfect twisting method does not fit the case (2), and there are significant errors at high frequencies. The result assuming a uniform field deviates from the results of 3-D FEM at high frequency, which is similar to the case (1). The impact of the longitudinal field is trivial in case (2). The difference in the impact of the longitudinal field between case (1) and case (2) comes from the structure. The strands in case (1) are twisted to achieve evenly spatial distributed radially and azimuthally. The angle between the strand and the z-axis varies at different locations. Therefore, the strand in case (1) is more likely to form a large angle between itself and other strands, and has a higher longitudinal field. Therefore, the impact of the longitudinal field in case (1) is more obvious. The proposed method is accurate in the whole frequency range. Fig. 9(b) and (d) shows the loss due to external magnetic field. The results do not show a significant difference. As the frequency increases, the error also slightly increases.

One important feature of Litz wire models is their computation speed. Table I gives the detail of 3-D FEMs and the computational time for two cases. The computation time includes modeling and solving for ten frequency points. The proposed method is several orders of magnitude faster than 3-D FEM, which takes less than 1 s to calculate each case.

TABLE I
NUMBERS OF ELEMENT AND COMPUTATION TIME OF 3-D FEMS AND THE PROPOSED METHOD FOR LITZ WIRES

Items	Case 1	Case 2
FEM number of element	104288	180807
FEM element average quality	0.5004	0.476
FEM used memory	20.42 GB	28.98 GB
FEM computation time	6360 s	8769 s
Proposed method number of element	180	220
Proposed method computation time	0.26 s	0.32 s

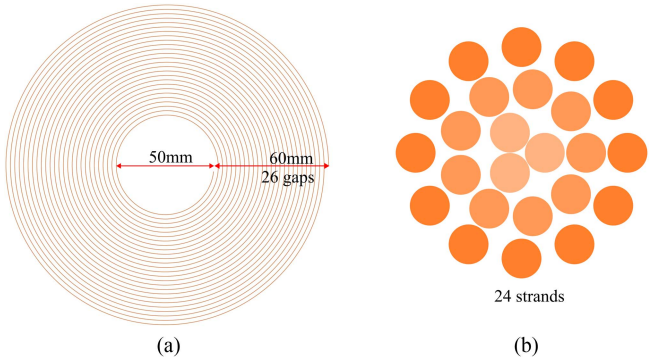

Fig. 10. Geometry of the air-core coil and used Litz wire.

B. Air-Core Coil

A planar coil is used to validate the equivalent element. Its geometry is shown in Fig. 10(a). The planar coil has 26 turns. Its inner radius is 25 mm, and the gap between turns is about 2.3 mm. The wire uses a one-level Litz wire, which has 24 strands

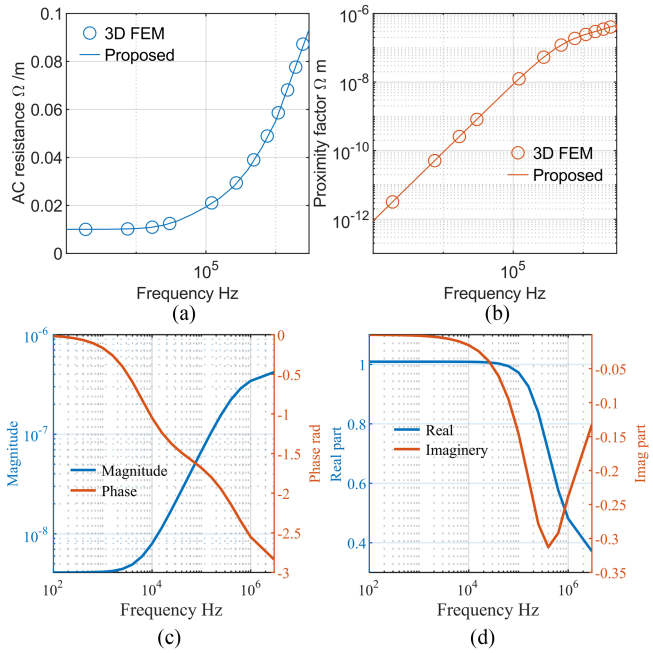

Fig. 11. Equivalent properties of Litz wire: (a) The AC resistance, (b) the proximity effect factor, (c) the ratio of $\dot{A}_1''$ to $\dot{A}_1'$, and (d) complex permeability.

with 0.3 mm diameter. The cross section is shown in Fig. 10(b). The pitch of the wire is 25 mm, and the outer radius a_o of the Litz wire is about 0.95 mm.

First, a pitch of the Litz wire is modeled with the proposed method and also verified with 3-D FEM. The model uses the same setting as the previous section. The results are shown in Fig. 11. Fig. 11(a) and (b) shows the results from 3-D FEM and proposed method. It confirms the accuracy of the results from the proposed method. Fig. 11(c) shows the factor Γ obtained from (20), and Fig. 11(d) shows the complex permeability $\dot{\mu}_{rc}$ obtained from Γ

$$\dot{\mu}_{rc} = \frac{1 + \Gamma/a_o^2}{1 - \Gamma/a_o^2}. \tag{21}$$

Then, the impedance of the coil is calculated by a 3-D model with cylindrical elements and 2-D axis-symmetry FEM with complex permeability. For the 3-D model with cylindrical elements, each turn is sectioned into 36 elements. The FEMs are built with COMSOL, and two different settings are used. One uses complex permeability from (21). Another is using homogenized complex permeability to replace the whole coil [19]. The details of the coil modeling are given in Table II. Besides, the coil sample, as shown in Fig. 12(a), is measured by Bode 100 in the frequency range from 100 Hz to 3 MHz.

Fig. 12(b) shows the reactance of the coil obtained from different methods. The reactances obtained in three different calculations almost overlap with the measurements. Fig. 12(c) and (d) shows the resistances obtained from different methods and their relative error compared to the measurement. The equivalent element shows good accuracy compared to the measurements, which validates the effectiveness of the equivalent element. The proposed method has better performance than the

TABLE II
NUMBER OF ELEMENTS AND COMPUTATION TIME OF FEMS AND THE PROPOSED METHOD FOR AIR-CORE COIL

Items	Litz wire	Air-core coil	
FEM Setting	3-D	2-Dax $\dot{\mu}_r$	2-Dax Homo $\dot{\mu}_r$
FEM number of element	614 098	1078	6183
FEM element average quality	0.5254	0.5263	0.5053
FEM used memory	40.06 GB	1.85 GB	2.21 GB
FEM computation time	37 678 s	4 s	7s
Proposed method number of element	480	1634	
Proposed method computation time	1.29 s	4.25 s	

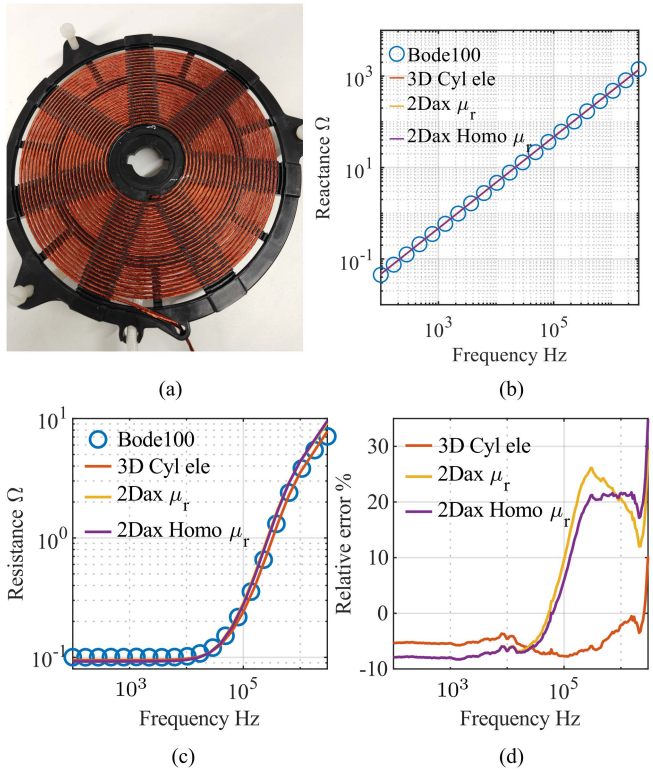

Fig. 12. (a) Photo of the measured coil, and comparison between measurement and calculation results from different methods, (b) reactance, (c) resistance, and (d) relative error of resistance.

results from 2-D axis-symmetry FEM. It keeps the relative error within 10% in the whole frequency range, which can conclude that the proposed method properly captures the eddy current feature in the coil. The error starts at a low frequency, which indicates the error comes from the dc resistance calculation. The reason could be the difference between the modeled and real structures of the Litz wire and coil, and the assumption that the current flow along the path of strands is not totally true. When the frequency approaches 3 MHz, the error has a fast change because it is close to the resonant point. For the results from the FEM, when the frequency is above 40 kHz, the resistance increases faster than the measurement. It leads to about 20%

overestimation when the frequency is above 100 kHz. The FEM with homogenized complex permeability has similar results as the equivalent complex permeability, and it shows the validation of homogenization.

In this section, the proposed method is validated through FEM and measurements. In all cases, the proposed method shows good accuracy and fast computation speed.

IV. Conclusion

A 3-D numerical impedance calculation method is proposed, which can be used to model Litz wires and air-core coils. The proposed method employs cylindrical elements, which results in a small amount of elements. Compared to other Litz wire model, the method considers the longitudinal field and the impact of eddy current in the transverse field. The equivalent cylindrical element is proposed to simplify the calculation for coils. The results from the proposed method have less than 10% error in a wide frequency range compared to FEM and measurements. Besides, its computational speed can be several orders of magnitudes faster than 3-D FEM. This proposed model shows promise in optimizing Litz wires and air-core coils.

Appendix
Detail of Transverse Field Analysis

In this appendix, some details of the 2-D transverse field analysis are provided to help understand the analysis. The magnetic vector potential inside the conductor is described by the following equation:

$$\nabla^2 A - j\omega\sigma\mu A = \mu\sigma\nabla\phi. \tag{22}$$

The general solution only considered the first harmonics is given in the following equation, where A_0 is the particular solution and is a constant here

$$A_{\mathrm{c}}(r,\varphi) = A_0 + \alpha_0 J_0(\kappa r) + J_1(\kappa r)(\alpha_1\cos\varphi + \beta_1\sin\varphi). \tag{23}$$

Then, the boundary conditions on the surface of the conductor are given in the following equation, where a is the radius of the round conductor:

$$\begin{aligned} \mu_{\mathrm{c}} H_{r\_\mathrm{c}}|_{r=a} &= \mu_0 H_{r\_\mathrm{air}}|_{r=a} \\ H_{\varphi\_\mathrm{c}}|_{r=a} &= H_{\varphi\_\mathrm{air}}|_{r=a} \\ A_{z\_\mathrm{c}}|_{r=a} &= A_{z\_\mathrm{air}}|_{r=a}. \end{aligned} \tag{24}$$

After equating the same harmonic terms in (2) and (23), the relationships in the following equation are obtained. Equation (3) is part of the following equation:

$$\begin{aligned} D &= -\frac{\mu_0 I}{2\pi} \quad \alpha_0 = -\frac{D}{\kappa a J_1(\kappa a)} \\ A_1''|B_1'' &= \frac{a^2 J_2(\kappa a)}{J_0(\kappa a)} A_1'|B_1' \\ \alpha_1|\beta_1 &= \frac{2}{\kappa a^2 J_2(\kappa a)} A_1''|B_1'' \\ cA_0 + \alpha_0 J_0(\kappa a) &= C + D\ln a. \end{aligned} \tag{25}$$

Equation (8) is obtained from integral (23) over the surface of the conductor. With the help of (25), (8) is obtained

$$\begin{aligned} \iint A_{\mathrm{c}} dS &= \int_0^a \int_0^{2\pi} A_{\mathrm{c}} r d\varphi dr \\ &= C + D\ln(a) - \frac{DJ_2(\kappa a)}{\kappa a J_1(\kappa a)}. \end{aligned} \tag{26}$$

References

[1] P. Czyz et al., "Analysis of the performance limits of 166 kW/7 kV air- and magnetic-core medium-voltage medium-frequency transformers for 1:1-DCX applications," *IEEE Trans. Emerg. Sel. Topics Power Electron.*, vol. 10, no. 3, pp. 2989–3012, Jun. 2022.

[2] T. Guillod, P. Czyz, and J. W. Kolar, "Geometrical optimization of medium-frequency air-core transformers for DCX applications," *IEEE Trans. Emerg. Sel. Topics Power Electron.*, vol. 10, no. 4, pp. 4319–4335, Aug. 2022.

[3] E. Plumed, I. Lope, C. Carretero, and J. Acero, "A recursive methodology for modelling multi-stranded wires with multilevel helix structure," *Appl. Math. Modelling*, vol. 83, pp. 76–89, Jul. 2020. [Online]. Available: https://linkinghub.elsevier.com/retrieve/pii/S0307904X20301050

[4] J. Ferreira, "Analytical computation of AC resistance of round and rectangular Litz wire windings," *IEE Proc. B. Electric Power Appl.*, vol. 139, no. 1, 1992, Art. no. 21. [Online]. Available: https://digital-library.theiet.org/content/journals/10.1049/ip-b.1992.0003

[5] C. C. R. Sullivan, "Optimal choice for number of strands in a Litz-wire transformer winding," *IEEE Trans. Power Electron.*, vol. 14, no. 2, pp. 283–291, Mar. 1999. [Online]. Available: https://ieeexplore.ieee.org/document/750181/

[6] F. Tourkhani and P. Viarouge, "Accurate analytical model of winding losses in round Litz wire windings," *IEEE Trans. Magn.*, vol. 37, no. 1, pp. 538–543, Jan. 2001.

[7] H. Rossmanith, M. Doebroenti, M. Albach, and D. Exner, "Measurement and characterization of high frequency losses in nonideal Litz wires," *IEEE Trans. Power Electron.*, vol. 26, no. 11, pp. 3386–3394, Nov. 2011. [Online]. Available: https://ieeexplore.ieee.org/document/5752256/

[8] C. R. Sullivan and R. Y. Zhang, "Analytical model for effects of twisting on Litz-wire losses," in *Proc. 2014 IEEE 15th Workshop Control Model. Power Electron.*, 2014, pp. 1–10. [Online]. Available: https://ieeexplore.ieee.org/document/6877187/

[9] T. Guillod, J. Huber, F. Krismer, and J. W. Kolar, "Litz wire losses: Effects of twisting imperfections," in *Proc. 2017 IEEE 18th Workshop Control Model. Power Electron.*, 2017, pp. 1–8. [Online]. Available: https://ieeexplore.ieee.org/document/8013327/

[10] T. Luo, M. G. Niasar, and P. Vaessen, "Fast 2.5-D loss calculation for round Litz wires," *IEEE Trans. Magn.*, vol. 60, no. 3, Mar. 2024, Art. no. 6300804. [Online]. Available: https://ieeexplore.ieee.org/document/10304281/

[11] S. Ehrlich, H. Rossmanith, M. Sauer, C. Joffe, and M. Marz, "Fast numerical power loss calculation for high-frequency Litz wires," *IEEE Trans. Power Electron.*, vol. 36, no. 2, pp. 2018–2032, Feb. 2021. [Online]. Available: https://ieeexplore.ieee.org/document/9138752/

[12] J. Lyu, H. C. Chen, Y. Zhang, Y. Du, and Q. S. Cheng, "Litz wire and uninsulated twisted wire assessment using a multilevel PEEC method," *IEEE Trans. Power Electron.*, vol. 37, no. 2, pp. 2372–2381, Feb. 2022.

[13] T. Ewald and J. Biela, "Analytical winding loss and inductance models for gapped inductors with Litz or solid wires," *IEEE Trans. Power Electron.*, vol. 37, no. 12, pp. 15127–15139, Dec. 2022. [Online]. Available: https://ieeexplore.ieee.org/document/9810506/

[14] K. Niyomsatian, J. Gyselinck, and R. V. Sabariego, "Closed-form complex permeability expression for proximity-effect homogenisation of Litz-wire windings," *IET Sci., Meas. Technol.*, vol. 14, no. 3, pp. 287–291, May 2020.

[15] Y. Otomo, H. Igarashi, H. Sano, and T. Yamada, "Analysis of Litz wire losses using homogenization-based FEM," *IEEE Trans. Magn.*, vol. 57, no. 8, Aug. 2021, Art. no. 7402409.

[16] T. Luo, M. G. Niasar, and P. Vaessen, "Two-dimensional frequency-dependent resistance and inductance calculation method for magnetic components with round conductors," *IEEE Trans. Magn.*, vol. 60, no. 1, Jan. 2024, Art. no. 8400211. [Online]. Available: https://ieeexplore.ieee.org/document/10345619/

[17] T. Luo, M. G. Niasar, and P. Vaessen, "Improved winding losses calculation based on Bessel functions," *IEEE Trans. Magn.*, vol. 59, no. 6, Jun. 2023, Art. no. 6300410.
[18] J. Gyselinck and P. Dular, "Frequency-domain homogenization of bundles of wires in 2-D magnetodynamic FE calculations," *IEEE Trans. Magn.*, vol. 41, no. 5, pp. 1416–1419, May 2005.
[19] H. Igarashi, "Semi-analytical approach for finite-element analysis of multi-turn coil considering skin and proximity effects," *IEEE Trans. Magn.*, vol. 53, no. 1, Jan. 2017, Art. no. 7400107. [Online]. Available: https://ieeexplore.ieee.org/document/7546864/

Tianming Luo (Student Member, IEEE) was born in Jinan, China, in 1993. He received the B.E. degree in electrical engineering and automation from Chongqing University, Chongqing, China, in 2015, and the M.Sc. degree in high voltage and insulation engineering from China Electric Power Research Institute, Beijing, China, in 2018. He is currently working toward the Ph.D. degree in electrical engineering with High Voltage Technologies Group, Delft University of Technology, Delft, The Netherlands.

His research interests include multiphysic models of medium-voltage medium-frequency transformers and insulation performance under medium frequencies.

Mohamad Ghaffarian Niasar (Member, IEEE) was born in Tehran, Iran, in 1984. He received the M.Sc. degree in electrical power engineering from the Sharif University of Technology, Tehran, in 2008, and the Ph.D. degree in electrical engineering from the Royal Institute of Technology (KTH), Stockholm, Sweden, 2015.

He is currently an Assistant Professor with High Voltage Technologies Group, Delft University of Technology, Delft, The Netherlands. His main research interests include aging of insulation material, HVdc insulation system, high-frequency power transformers, and multiphysics modeling of power components.

Peter Vaessen (Member, IEEE) was born in Maasbree, The Netherlands, in 1960. He received the M.Sc. degree (cum laude) in electrical power engineering from Eindhoven Technical University, Eindhoven, The Netherlands, in 1985.

In 1985, he joined KEMA (currently a CESI brand). In his 35-year career, he held research positions in the field of large power transformers and high-voltage measurement and testing. He has 25 years of experience in (U)HVdc technology and T & D grids with high shares of renewables. He is the Manager of innovations with KEMA Laboratories and the Chairman of the European Distributed Energy Resources Laboratories association (DERlab), as well as Member of several national and international working groups. Since 2017, he has been a part-time Professor of hybrid transmission systems with TU Delft, where he teaches high-voltage technology and HVdc.